THE JOURNAL OF PHYSICAL CHEMISTRY A
A JOURNAL OF THE AMERICAN CHEMICAL SOCIETY

pubs.acs.org/JPCA

Article

Site-Specific Assignments of C−H and C−D Vibrations in Gaseous 1-Butanol by High-Resolution Cavity-Enhanced Raman Spectroscopy

Yuanqin Yu, Chongyan Shi, Qingying Yang, Yan Tan,* and Shuiming Hu

Cite This: *J. Phys. Chem. A* 2026, 130, 2523−2532

Read Online

ACCESS | Metrics & More | Article Recommendations | Supporting Information

ABSTRACT: C−H and C−D vibrations serve as versatile Raman probes for molecular detection and structural characterization, while site-specific vibrational analysis remains challenging due to overlapping modes and complex isotope effects. 1-Butanol ($CH_3CH_2CH_2CH_2OH$), a model small molecule with four distinct C−H moieties along its carbon chain, offers an ideal platform to decipher such complexity—yet the assignment of its gas-phase vibrational spectra (including Fermi resonances and site-dependent modes) has long been hindered by insufficient spectral resolution. Using a sensitive cavity-enhanced Raman instrument developed recently, we recorded high-resolution gas-phase Raman spectra of 1-butanol and two selectively deuterated isotopologues ($CH_3CD_2CD_2CD_2OH$ and $CD_3CD_2CD_2CH_2OH$) in the ranges of 900−3100 cm^{-1}, covering both C−H/C−D bending and stretching regions. By integration of quantum chemical calculations, isotope substitution, and polarization-dependent measurements, the spectral ambiguities were unraveled. Our analysis enables the assignments of all major spectral features, elucidating the role of symmetric and antisymmetric stretching vibrations and Fermi-resonant modes at each C−H site along the 1-butanol carbon chain. A systematic comparison of C−H versus C−D vibrational patterns allows us to quantify isotope-induced shifts in frequency and intensity. These findings not only advance fundamental understanding of 1-butanol's vibrational landscape but also provide a robust framework for site-specific Raman analysis of complex organic molecules and guide the design of Raman-based imaging probes for biological and environmental applications.

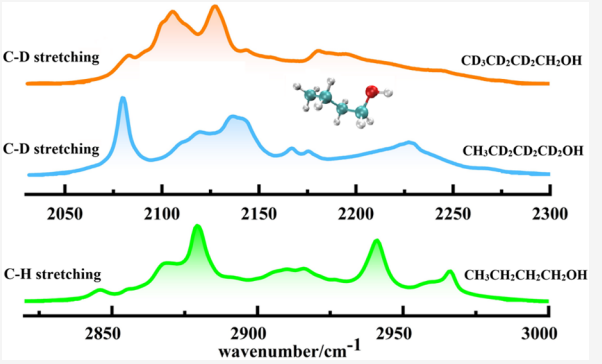

1. INTRODUCTION

Raman spectroscopy, which captures unique molecular fingerprints, is one of the most versatile analytical tools across diverse scientific fields, including physics, chemistry, biology, materials science, and pharmaceutical engineering. The recent emergence of nonlinear Raman techniques has further expanded its reach. The structural and dynamical information on molecules can be revealed from Raman spectra. Consequently, establishing an accurate correlation between the observed spectral features and their corresponding vibrational modes is crucial for subsequent applications.

Many functional groups have been established as a Raman probe, such as the −CH group, hydroxyl group (−OH), carbonyl group (−C═O), amide group ($-CONH_2$), and nitrile group (−C≡N). Among them, the −CH group is particularly important since it is ubiquitous in organic and biological molecules. Moreover, C−H vibration is highly sensitive to molecular structures, intermolecular interactions, and local environments.[1−8] These features render the C−H spectra attractive, especially in the C−H stretching region between 2800 and 3100 cm^{-1}. For instance, the C−H stretching vibration is one of the most frequently employed probes in the sum-frequency generation (SFG) spectroscopy at interface and in stimulated Raman scattering (SRS) microscopy for real-time imaging within biological cells.[9−13]

Despite the role of C−H vibrations, their assignments are challenging. First, molecules often contain several C−H types, such as methyl ($-CH_3$), methylene ($-CH_2$), and methine (−CH) groups. Spectral features can even vary for the same group type depending on its position along a carbon chain (e.g., α-CH_2, β-CH_2, and γ-CH_2). This limits the ability of C−H spectra to discriminate molecular species rich in methylene groups. For example, coherent Raman imaging of lipophilic compounds often relies on a single vibrational mode, the methylene symmetric stretch at ∼2845 cm^{-1}, highlighting this limitation.[9] Second, the C−H stretching region is congested with multiple modes, including symmetric and antisymmetric

Received: December 10, 2025
Revised: March 3, 2026
Accepted: March 4, 2026
Published: March 11, 2026

Downloaded via UNIV SCIENCE AND TECHNOLOGY CHINA on March 27, 2026 at 02:58:06 (UTC).
See https://pubs.acs.org/sharingguidelines for options on how to legitimately share published articles.

© 2026 American Chemical Society

https://doi.org/10.1021/acs.jpca.5c08365
J. Phys. Chem. A 2026, 130, 2523−2532

stretches and the coupled Fermi resonance (FR) modes, which complicates a comprehensive spectral interpretation. Several force fields and ab initio calculation models have been developed to decipher complex C−H spectra as a result of Fermi resonance.[14−20] For example, Sibert and co-workers developed a first-principles model for describing the Fermi resonance in the alkyl CH stretching region based on a local mode Hamiltonian that incorporates cubic stretch−bend coupling.[17] Alternative theoretical treatment on the Fermi resonance of methyl-groups has been attempted by Kuo and co-workers using an ab initio calculation based on quartic potential generated at the MP2/aug-cc-pVDZ level and the corresponding eigenvalue problem was solved by the vibrational configurational interaction (VCI) method.[18,19] Recently, an anharmonic local mode analysis of cyclohexane provided an interpretation of the C−H stretching spectrum, demonstrating that Fermi resonance coupling terms are essential for a physical insight into the vibrational energy levels.[21]

Deuteration isotope substitution severs as another way to resolve complex C−H spectra since it moves the stretching spectra from 2800−3100 cm^{-1} to a so-called silent region at 2000−2300 cm^{-1}, which is separated from almost all Raman peaks of organic compounds. Consequently, spectral overlap is minimized by using selectively deuterated samples, enabling clear identification of the individual contributions from various C−H groups.[4] Furthermore, the C−D vibration itself functions as a versatile Raman tag for tracking structural changes and dynamics in labeled compounds, particularly drugs and biomolecules.[22−24] Compared to conventional fluorescent tags, deuteration labeling offers distinct advantages, including negligible toxicity to biological samples and minimal steric perturbation of the system under study. Deuteration can also enhance drug half-life and reduce membrane peroxidation of unsaturated fatty acids.[25] Given these applications, establishing a precise correspondence between the observed C−D peaks and their vibrational modes is also highly desirable.

Previous studies of the C−H and C−D spectra of organic molecules have primarily relied on liquid-phase Raman or infrared spectroscopy. However, intermolecular interactions in the condensed phase significantly broaden and distort the spectral bands. As a result, many fine spectral details are obscured, which has led to frequent misassignments that have even been used to interpret some important dynamical processes.[26,27] In contrast, gas-phase Raman spectroscopy is free from such complications due to the absence of intermolecular interactions. Moreover, gas-phase Raman spectra typically exhibit narrower band profiles compared with their gas-phase infrared counterparts. This is because gas-phase IR spectra consist of P, Q, and R branches, while Raman spectra are dominated by a sharp Q branch, resulting in an intrinsically higher resolution. Well-assigned gas-phase Raman spectra can thus provide a critical reference for interpreting their liquid-phase counterparts and for evaluating the external factors that perturb intermolecular interactions in the liquid state. However, the widespread application of gas-phase Raman spectroscopy has been limited by its inherently low sensitivity, a consequence of small Raman scattering cross sections, resulting in a scarcity of high-quality reported spectra.[28−31] Recently, using a cavity-enhanced instrument that combines high-precision locking technology, we improved the detection limit for gas-phase Raman measurements to the subppm level.[32] Such high sensitivity allows the convenient acquisition of gas-phase Raman spectra, even for organic compounds with low saturation vapor pressures such as the 1-butanol investigated here.

1-Butanol ($CH_3CH_2CH_2CH_2OH$) is an excellent model system for investigating C−H/C−D spectra due to its small size and the presence of four distinct C−H groups: a terminal CH_3, and α-, β-, and γ-CH_2 groups. Each group experiences a different chemical environment along the carbon chain, providing key insights into site-specific spectral signatures. In previous studies, several vibrational spectroscopic methods have been employed to investigate the C−H spectra of 1-butanol, including gas-phase and liquid infrared spectroscopy, low-temperature matrix infrared spectroscopy, SFG spectra, and liquid Raman spectroscopy.[33−40] However, a clear assignment has remained lacking, and high-resolution gas-phase Raman data have been unavailable. For this end, we measured and analyzed gas-phase Raman spectra of 1-butanol and its two deuterated samples in the range 900−3100 cm^{-1}, which covers the C−H/C−D bending and stretching regions.

Finally, the growing role of artificial intelligence (AI) and machine learning (ML) in spectral prediction, analysis, and application should be noted. For instance, deep learning models have recently been developed to predict the spectra of series of organic molecules with improved efficiency and accuracy.[41,42] The ML models require reliable data sets for training and validation. In this context, the well-assigned, high-resolution gas-phase Raman spectrum of a model molecule such as 1-butanol serves as an ideal benchmark for developing such tools. Experimental data validate the accuracy of calculation and help to further improve theoretical models, which in turn provides stronger support for interpreting more complex experimental spectra.

2. EXPERIMENTAL AND COMPUTATIONAL METHODS

Deuterated 1-butanol, $CH_3CD_2CD_2CD_2OH$, and $CD_3CD_2CD_2CH_2OH$ were purchased from ICON isotopes (98%). Normal 1-butanol ($CH_3CH_2CH_2CH_2OH$) was obtained from Aladin (99.8%, GC grade).

The gas-phase Raman spectra were acquired using a home-built cavity-enhanced Raman spectrometer, the details of which have been described elsewhere.[32] Briefly, the excitation source was a 1064 nm fiber laser, the output of which was frequency-doubled to generate a 532 nm radiation. For polarization-resolved measurements, the 532 nm beam was linearly polarized using a Glan-laser polarizer and coupled into a high-finesse Fabry−Pérot cavity after passing a group of lenses. This Fabry−Pérot cavity, comprising two high-reflectivity mirrors, was housed within a stainless-steel vacuum chamber and had a length of 72 cm, corresponding to a free spectral range (FSR) of approximately 208 MHz. The laser frequency was stabilized to a longitudinal mode of the cavity using the Pound−Drever−Hall (PDH) locking technique, yielding an estimated intracavity circulating power of 300 W. The forward-scattered Raman signal was collected by a 100 mm focal length lens and dispersed by a grating spectrometer (Andor SR-750, 1200 grooves/mm) equipped with a liquid-nitrogen-cooled charge-coupled device (CCD) camera (Andor DV401A-BVF, 200−1100 nm response).

All quantum chemical calculations were performed using the Gaussian 16 program package.[43] Geometry optimizations and harmonic vibrational frequency calculations were conducted at the B3LYP-D3/6-311++G(d,p) level of theory with zero-point energy (ZPE) corrections included. To locate the 14 conformers of 1-butanol, an initial conformational search was performed using the semiempirical PM7 method based on the Molclus code.[44] The resulting structures were subsequently reoptimized at the B3LYP-D3/6-311++G(d,p) level. To achieve more accurate relative energies, single-point energy calculations were carried out at the MP2/aug-cc-

https://doi.org/10.1021/acs.jpca.5c08365
J. Phys. Chem. A 2026, 130, 2523−2532

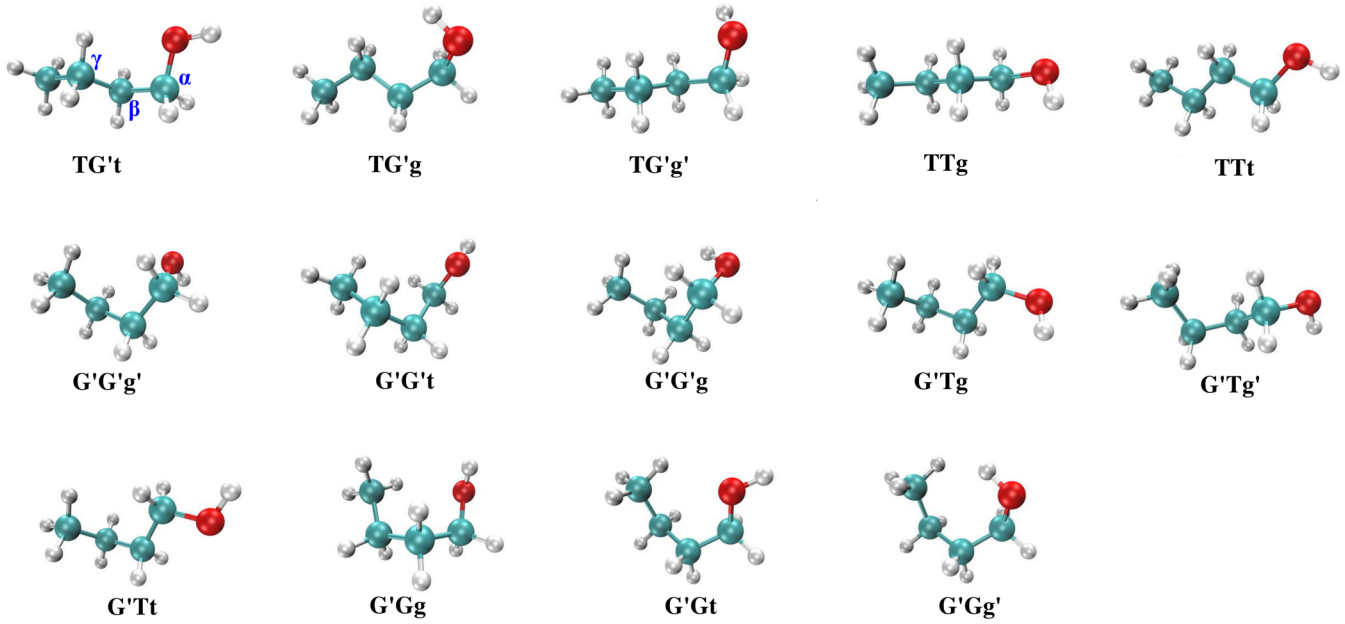

Figure 1. Calculated geometry for 14 conformers of 1-butanol.

pVTZ level by using the B3LYP-D3/6-311++G(d,p) optimized geometries and ZPEs. The Boltzmann population factors (F) for the conformers at 298.15 K were calculated using the Shermo program (version 2.3.5) based on the Gibbs free energy (ΔG) at the MP2/aug-cc-pVTZ level,[45] according to eq 1

$$F_i = \frac{\exp(-\Delta G_i/RT)}{\sum \exp(-\Delta G_i/RT)} \times 100\% \quad (1)$$

where ΔG_i is the relative free energy of conformer "i" which is relative to the lowest-energy conformer, T is the temperature in Kelvin at room temperature (298.15 K), and R = 0.00199 kcal/(mol·K) is the Boltzmann constant.

Harmonic calculations are insufficient to describe Raman spectrum of 1-butanol in the C−H and C−D stretching region since the C−H and C−D stretching fundamental transitions are nearly degenerate with overtone bands of bending modes, borrowing intensity through Fermi resonances. In order to overcome the disagreement between harmonic frequencies and experimental data and to avoid using the scaled frequency factor, we therefore used second-order vibrational perturbation theory (VPT2) calculations to assist the assignment of experimental spectrum in the range of 900−3100 cm^{-1},[46] employing the same functional and basis sets as for the harmonic frequency and structure optimization with B3LYP-D3/6-311++G(d,p) by Gaussian 16.

3. RESULTS AND DISCUSSIONS

3.1. Calculated Structures

1-Butanol has rich conformational distributions, which may affect the spectral features to some extent. A detailed analysis of its conformers was therefore performed, as presented in Figure 1. The 1-butanol molecule possesses 3 principal dihedral angles defined by the C−C−C−C, C−C−C−O, and C−C−O−H atoms, which give rise to 14 distinct conformations. These conformers can be categorized into five families: TG′x, TTx, G′G′x, G′Tx, and G′Gx. In this nomenclature, the uppercase letters (T, G) denote the approximate dihedral angles of the C−C−C−C and C−C−C−O backbones, while the subscript lowercase letter x (which can be t, g, or g′) specifies the C−C−O−H dihedral angle. Here, T and t correspond to a trans conformation (∼180°), G and g to a gauche arrangement (∼+60°), and the prime (′) indicates a negative dihedral angle (∼−60°). Except for the TTx family, each other family comprises three conformers corresponding to x = t, g, and g′. The TTx family contains only two unique conformers, as TTg and TTg′ are structurally equivalent. The statistical weight is 1 for the TTt conformer, whereas those are 2 for all other 13 conformations.

Table 1 summarizes the calculated relative energies and Boltzmann factors for 14 conformers of 1-butanol, where the global minimum energy structure of TG′t was set to zero. The summed Boltzmann factors of the five lowest-energy conformers—belonging to the TG′x and TTx families—account for 67.2% of the total at room temperature. This indicates that these conformers are the predominant species under

Table 1. Calculated Relative Energies ΔE (kJ/mol) for 14 Conformers of 1-Butanol along with the Boltzmann Factors (F)

conformer	ΔE[a]	F (%)[b]
TG′t	0	21.8
TG′g′	0.26	11.4
TG′g	0.42	12.1
TTg	0.57	12.4
TTt	0.70	9.5
G′G′g′	1.87	5.2
G′G′t	1.94	8.6
G′G′g	2.57	4.2
G′Tg′	3.10	3.6
G′Tg	3.46	3.1
G′Tt	3.57	5.1
G′Gg	5.16	0.9
G′Gt	5.38	1.3
G′Gg′	7.00	0.4

[a]Calculated at MP2/aug-cc-pVTZ// B3LYP-D3/6-311++G(d,p) level. [b]Boltzmann populations obtained from Gibbs free energy (ΔG) calculated by MP2/aug-cc-pVTZ electronic energies with ZPE using B3LYP-D3/6-311++G(d,p) at 298 K.

https://doi.org/10.1021/acs.jpca.5c08365
J. Phys. Chem. A 2026, 130, 2523−2532

experimental conditions and, consequently, the primary contributors to the observed gas-phase Raman spectra. Among above five conformers, the most stable conformer, TG′t, has a calculated population of 21.8%, which is approximately twice that of the other four conformers of TG′g′ (11.4%), TG′g (12.1%), TTg (12.4%), and TTt (9.5%), respectively, as seen from Table 1. Therefore, to simplify the spectral assignment, the calculated vibrational frequencies and Raman activities of the most stable conformer of TG′t were used as a guide for interpreting experimental spectra. The corresponding data for the other four low-energy conformers are provided in the Supporting Information (Figures S1−S3). As seen from Figures S1−S3, for the same kind of vibrations, the calculated CH_3 frequencies show almost no differences among the first five low-energy conformers, whereas for the α-CH_2, β-CH_2, and γ-CH_2, they exhibit some conformational dependencies but the frequency differences are generally within 10 cm^{-1}.

3.2. Gas-Phase Raman Spectra of 1-Butanol

3.2.1. C−H and C−D Bending Regions. Raman bands in the fingerprint region exhibit intensities nearly 10 times lower than those in the stretching region. Benefited from high sensitivity of the cavity-enhanced Raman spectroscopy employed in this work, we successfully recorded these low-intensity signals. Figure 2 displays the polarized and depolarized gas-phase Raman spectra of normal 1-butanol in the 900−1600 cm^{-1} fingerprint region, together with the polarized spectra of the two deuterated isotopologues ($CH_3CD_2CD_2CD_2OH$ and $CD_3CD_2CD_2CH_2OH$). The use of selectively deuterated samples allows for the discrimination of the spectral contributions of different sites along the carbon chain. For each species, the calculated anharmonic frequencies and Raman activities are plotted according to the most stable TG′t conformer. To achieve visual clarity, the spectral contributions of four distinct C−H groups are color-coded in subsequent figures as follows: blue for α-CH_2, green for β-CH_2, dark yellow for γ-CH_2, and pink for the terminal CH_3 group, as presented in Figure 2.

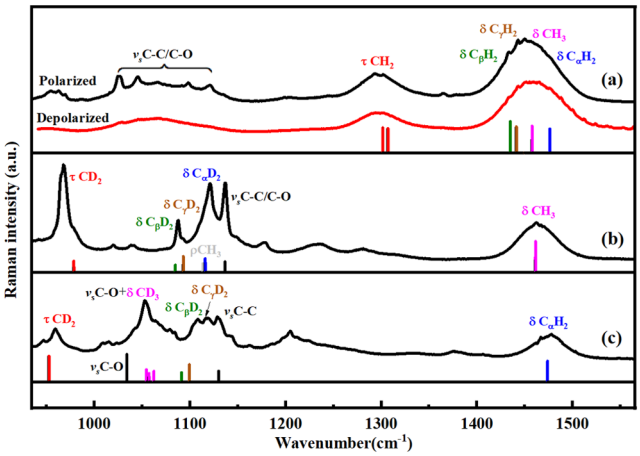

Figure 2. Gas-phase Raman spectra in the bending region (900−1600 cm^{-1}) for 1-butanol and its two deuterated isotopologues along with the predicted anharmonic frequencies and Raman intensities for the most stable conformer (TG′t). (a) Polarized and depolarized spectra of normal 1-butanol ($CH_3CH_2CH_2CH_2OH$). (b) Polarized spectrum of $CH_3CD_2CD_2CD_2OH$. (c) Polarized spectrum of $CD_3CD_2CD_2CH_2OH$. The spectral assignments are color-coded as follows: the blue for α-CH_2, the green for β-CH_2, the dark yellow for γ-CH_2, and the pink for CH_3. δ: scissoring vibration; τ, twisting vibration; ρ, rocking vibration.

We first focus on the C−H bending region (1300−1600 cm^{-1}). As seen from Figure 2b,c, both deuterated $CH_3CD_2CD_2CD_2OH$ and $CD_3CD_2CD_2CH_2OH$ exhibit a broad band in the range of 1400−1500 cm^{-1}, which is centered at 1464 and 1478 cm^{-1}, respectively. According to the calculations, these two bands can be assigned to the CH_3 and α-CH_2 scissoring vibrations, labeled as δCH_3 and $\delta C_\alpha H_2$, where δ denotes the scissoring vibration. Furthermore, comparing normal 1-butanol with two deuterated samples in the same spectral region, it is evident that the spectra show a noticeable frequency shift of the band center toward lower wavenumber while the bandwidth has increased significantly, as shown in Figure 2a. This change can be attributed to the contributions of $\delta C_\beta H_2$ and $\delta C_\gamma H_2$. To show their contributions, the experimental spectra were fitted with four Lorentz bands, of which two bands have a fixed position and width as in the case of $CH_3CD_2CD_2CD_2OH$ and $CD_3CD_2CD_2CH_2OH$ and the other two are unconstrained, the results of which are presented in Figure 3a. Clearly, the spectra could be deconvoluted into four bands as expected. Thus, the $\delta C_\beta H_2$ and $\delta C_\gamma H_2$ were determined at 1431 and 1447 cm^{-1}, in whole agreement with the calculated positions at 1435 and 1441 cm^{-1}, respectively. Therefore, the observed C−H scissoring

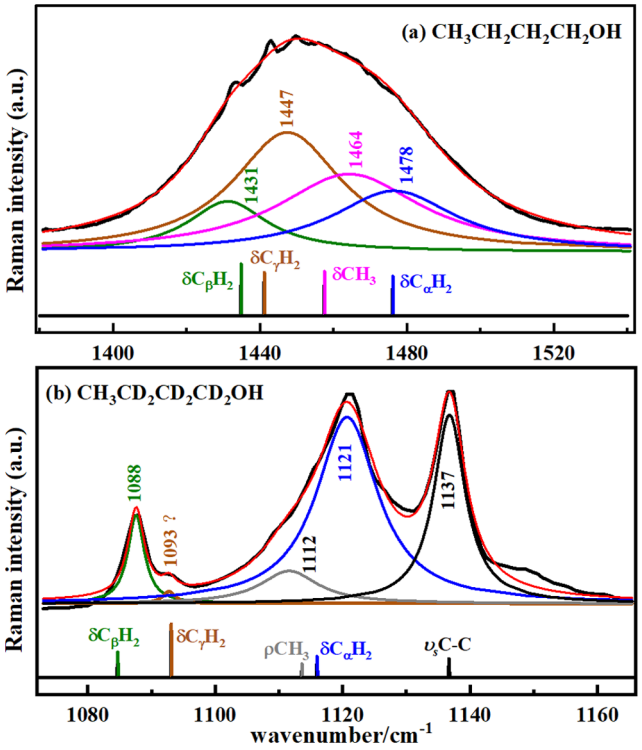

Figure 3. (a) Experimental and fitted (solid red line) gas-phase Raman spectra of normal 1-butanol in the C−H bending region (1400−1500 cm^{-1}), (b) the experimental and fitted (solid red line) gas-phase Raman spectra of deuterated 1-butanol in the C−D bending region (1070−1170 cm^{-1}). The predicted anharmonic C−H/C−D frequencies and Raman intensities are also plotted. Both spectra are fitted with Lorentz line shape functions. The components are color-coded as follows: the blue for α-CH_2, the green for β-CH_2, the dark yellow for γ-CH_2, and the pink for CH_3. δ: scissoring vibration; ρ: rocking vibration.

https://doi.org/10.1021/acs.jpca.5c08365
J. Phys. Chem. A 2026, 130, 2523−2532

Table 2. Observed Band Positions (cm^{-1}) of the Main Vibrational Modes and Their Assignments in Normal and Deuterated 1-Butanol

				isotopic shift ratio	
vibrational modes[a]	$CH_3(CH_2)_3OH$	$CH_3(CD_2)_3OH$	$CD_3(CD_2)_2CH_2OH$	exp	cal
$\tau(CH_2/CD_2)$	1300	970	960	1.34/1.35	1.33/1.36
$\delta(CH_3/CD_3)$	1464	1464	1054	1.39	1.38
$\delta(C_\alpha H_2/C_\alpha D_2)$	1478	1121	1478	1.32	1.32
$\delta(C_\beta H_2/C_\beta D_2)$	1431	1088	1107	1.32/1.29	1.32/1.31
$\delta(C_\gamma H_2/C_\gamma D_2)$	1447	1093	1119	1.32/1.29	1.33/1.32
$\upsilon_{as}(CH_3/CD_3)$	2963	2967	2227	1.33	1.32
$\upsilon_s(CH_3/CD_3)$	2879	2879	2080	1.38	1.39
$\upsilon_s(C_\alpha H_2/C_\alpha D_2)$	2870	2083	2876	1.38	1.38
$\upsilon_s(C_\beta H_2/C_\beta D_2)$	2846	2105	2119	1.35/1.34	1.36/1.36
$\upsilon_s(C_\gamma H_2/C_\gamma D_2)$	2856	2127	2136	1.34/1.34	1.35/1.35
$FR(CH_3/CD_3)$	2941	2938	2143	1.37	1.39
$FR(C_\alpha H_2/C_\alpha D_2)$	2963	2245	2965	1.32	1.32
$FR(C_\beta H_2/C_\beta D_2)$	2910	2181	2167	1.33/1.34	1.34/1.33
$FR(C_\gamma H_2/C_\gamma D_2)$	2916	2196	2176	1.33/1.34	1.34/1.33

[a] τ: twisting vibration; δ: scissoring vibration; υ: stretching vibration; FR: Fermi resonance.

vibrations of 1-butanol follow the descending frequency order: $\delta C_\alpha H_2 > \delta CH_3 > \delta C_\gamma H_2 > \delta C_\beta H_2$, with a maximum difference of approximately 47 cm^{-1}. Additionally, a medium-intensity band at ~1300 cm^{-1} in Figure 2a is assigned to the in-phase CH_2 twisting mode (τCH_2), in which all CH_2 groups twist cooperatively in the same direction (see the corresponding atomic displacements in Figure S4).

We now turn to the assignments in the lower-frequency region (900−1300 cm^{-1}), which covers C−D scissoring, rocking, and twisting vibrations as well as the C−C/C−O stretching. Therefore, the spectral identifications within this range becomes very complex due to the mixing of various vibrations. As shown in Figure 2a, several bands are observed in 900−1300 cm^{-1} range for normal 1-butanol, e.g., at 1026, 1045, 1098, and 1120 cm^{-1}, which are assigned to the coupled C−C and C−O stretching motions, labeled as ν_sC−C and ν_sC−O.

For deuterated $CH_3CD_2CD_2CD_2OH$, all of the CH_2 groups of normal 1-butanol are replaced by the CD_2. As seen from Figure 2b, upon deuteration, some C−C/C−O stretching vibrations are no longer clearly visible due to the coupling with the CD_2 bending vibrations. To obtain individual contributions of three CD_2, the observed Raman spectra between 1070 and 1170 cm^{-1} were fitted with five Lorentz line shape functions based on the calculated results, as shown in Figure 3b. By contrasting to the calculations, the fitted component at 1137 cm^{-1} can be assigned to the ν_sC−C/C−O which is mixed with some CD_2 scissoring vibrations according to the atomic displacements by GaussianView software, whereas the components at 1121, 1112, 1093, and 1088 cm^{-1} can correspond to the $\delta C_\alpha D_2$, ρCH_3, $\delta C_\gamma D_2$, and $\delta C_\beta D_2$, respectively, where ρ represents the CH_3 rocking vibration. With such an assignment, it seems that the predicted anharmonic band positions are consistent with the observed ones. However, the intensity ordering between $\delta C_\gamma D_2$ and $\delta C_\beta D_2$ is exactly reversed with a large deviation. Therefore, another possibility exists that the $\delta C_\gamma D_2$ and $\delta C_\beta D_2$ overlap to give rise to one peak due to their close frequencies. In addition, a strong low-frequency band at 970 cm^{-1} was assigned to the in-phase twisting vibration of three CD_2 groups in $CH_3CD_2CD_2CD_2OH$, which lied at 1300 cm^{-1} in normal $CH_3CH_2CH_2CH_2OH$. In previous studies on deuterated long-chain hydrocarbon, the identification of 970 cm^{-1} band has been confused. It was initially assigned to a CD_2 scissoring mode in early work but was recently reassigned to a C−C stretching vibration in the all-trans conformation, serving as a conformational marker.[22,23,47]

For the deuterated sample of $CD_3CD_2CD_2CH_2OH$ in Figure 2c, it gives very complex band shape in the range of 1000−1200 cm^{-1}. Unlike the case in $CD_3CD_2CD_2CH_2OH$, it is difficult to deconvolute the spectra into several Lorentz bands based on the calculated results. Contrasting to the calculations, we assign the prominent band at 1054 cm^{-1} to the symmetric CD_3 scissoring vibrations (δCD_3), which superimposes the C−O stretching vibration, as seen from Figure 2c. The increased isotopic mass lowers the CD3 bending frequency relative to that of CD_2. For the bands at 1129, 1119, and 1107 cm^{-1}, it can be attributed to ν_sC−C/C−O, $\delta C_\gamma D_2$, and $\delta C_\beta D_2$, respectively, while the band at 960 cm^{-1} is attributed to τCD_2 vibration.

The assignments of the main vibrational modes in the C−H and C−D bending regions are collected in Table 2, in which the frequencies corresponding to the same C−H and C−D vibrations are compared. Experimental isotopic shift ratios are in good agreement with the calculated isotopic shift ratios, indicating a correct association between them.

3.2.2. C−H Stretching Region. Figure 4 presents the polarized and depolarized Raman spectra of gaseous 1-butanol in the C−H stretching region (2800−3100 cm^{-1}), along with the polarized spectra of the two deuterated samples. A dramatic contrast is observed between the polarized and depolarized spectra in Figure 4a. The polarized spectrum exhibits many well-resolved bands, whereas the depolarized spectrum is characterized by a weak and broad profile. This indicates that the well-resolved bands in the polarized spectrum arise from totally symmetric vibrational modes, while the depolarized spectrum is dominated by antisymmetric ones. It is known that the weak intensity of the depolarized spectrum is inherent to Raman spectroscopy, as antisymmetric stretches typically exhibit low Raman scattering cross sections but are strong in IR absorption due to different selection rules. Furthermore, the broad spectral features can be explained by the rotational branch structure. For the antisymmetric modes of depolarization ratio $\rho \sim 0.75$, the Raman transitions involve

https://doi.org/10.1021/acs.jpca.5c08365
J. Phys. Chem. A 2026, 130, 2523−2532

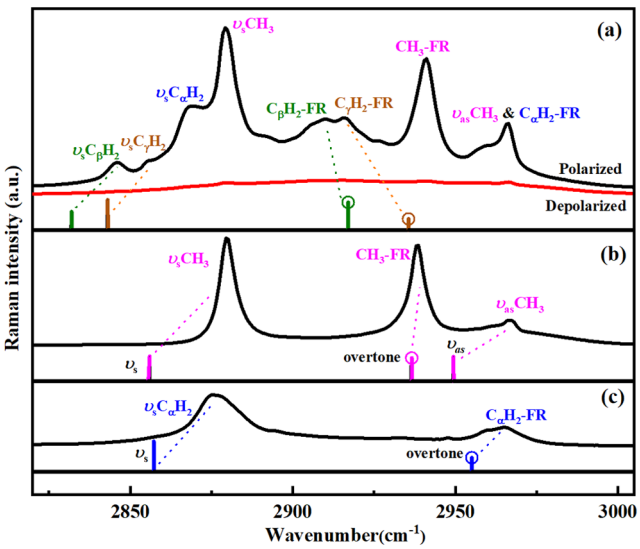

Figure 4. Gas-phase Raman spectra of 1-butanol in the C−H stretching region (2800−3100 cm^{-1}) along with the predicted C−H Fermi resonance pairs by VPT2 method. (a) Polarized and depolarized spectra of normal 1-butanol ($CH_3CH_2CH_2CH_2OH$). (b) Polarized spectrum of $CH_3CD_2CD_2CD_2OH$. (c) Polarized spectrum of $CD_3CD_2CD_2CH_2OH$. Spectral assignments are color-coded as follows: the blue for α-CH_2, the green for β-CH_2, the dark yellow for γ-CH_2, and the pink for CH_3. υ_s: stretching vibration; FR, Fermi resonance. A line with a circle above it denotes the overtone after the Fermi resonance interaction. It should be mentioned that for the $CH_3CD_2CD_2CD_2OH$, only the calculated symmetric in-plane $\upsilon_{as}CH_3$ is plotted, whereas the antisymmetric out-of-plane $\upsilon_{as}CH_3$ is not.

P, Q, and R branches ($\Delta J = \pm 1, 0$), while for the symmetric modes, the Raman transitions are dominated by the Q branch ($\Delta J = 0$). The closer the depolarization ratio is to 0, the more dominant the Q branch becomes.

It should be mentioned that the depolarized spectra were not measured for two deuterated 1-butanol due to the limited quantity of our isotope samples. However, as the isotope substitution employed here does not alter the symmetric properties of vibrational modes of 1-butanol, the well-resolved bands in two deuterated samples (Figure 4b,c) should also belong to symmetric categories. Therefore, considering that all major prominent Raman peaks originate from symmetric modes, we plotted only the calculated C−H symmetric stretching vibrations (υ_s) in Figure 4a−c, whereas the antisymmetric stretches (υ_{as}) are omitted, except for $\upsilon_{as}CH_3$, for reasons detailed below.

As mentioned earlier, Fermi resonance (FR) generally occurs between the stretching fundamental and the first overtone of a bending mode when they are close in frequency and share the same symmetry. This interaction leads to intensity borrowing by the overtone and a mixing of the wave functions between the fundamental and the overtone, resulting in one component to a lower frequency and the other to a higher frequency. The involvement of the FR significantly increases spectral complexity and is a major source of misassignment in C−H spectra. While theoretical calculations can predict relatively reliable fundamental band positions, accurately modeling FR interactions remains challenging.[14−21,48] To guide the assignment of experimental spectra, the calculated Fermi resonance pairs using the VPT2 method are plotted in Figure 4.

As seen from Figure 4b,c, for two deuterated samples of $CH_3CD_2CD_2CD_2OH$ and $CD_3CD_2CD_2CH_2OH$, the anharmonic prediction on the band positions and Raman intensities of CH_3 and α-CH_2 Fermi resonance pairs are in good agreement with the observed gas-phase Raman spectra, although it underestimates the frequency of Fermi resonance pairs as a whole. According to the calculations, for $CD_3CD_2CD_2CH_2OH$, a pair of peaks at 2876 and 2965 cm^{-1} was assigned to α-CH_2 Fermi resonance pairs labeled as $\upsilon_sC_\alpha H_2$ and FR-$C_\alpha H_2$, respectively, whereas for the $CH_3CD_2CD_2CD_2OH$, the two very strong bands at 2879 and 2938 cm^{-1} was assigned to the CH_3 Fermi resonance pair of υ_sCH_3 and FR-CH_3, and another weak band at 2967 cm^{-1} corresponds to the CH_3 in-plane antisymmetric stretching ($\upsilon_{as}CH_3$).

It should be especially mentioned that for the α-CH_2, the 2965 cm^{-1} band was assigned to $C_\alpha H_2$ symmetric stretching of different conformers in liquid Raman spectra on monohydric alcohol in previous study.[49] Here, our VPT2 calculations on 1-butanol indicate that this band originates from the α-CH_2 Fermi resonance, as shown in Figure 4c. Comparing spectral features of CH_3 and α-CH_2 in two deuterated samples, the α-CH_2 bands are much broader than those of CH_3. This is in good agreement with the calculations that the α-CH_2 vibration is more sensitive to molecular conformation$_3$, leading to band broadening due to the superposition of multiple conformers and an observable weak band at 2895 cm^{-1}, as illustrated in Figure S2. In recent studies, it is also shown that the C−H stretching vibration can be used a probe for the conformations of phenylalanine.[50]

As for why the $\upsilon_{as}CH_3$ mode appears in the polarized spectra with an observable intensity in $CH_3CD_2CD_2CD_2OH$ while the $\upsilon_{as}CH_2$ does not be assigned in $CD_3CD_2CD_2CH_2OH$, this can be attributed to the fact that the CH_3 group possesses two nearly degenerate antisymmetric stretching vibrations with different symmetries: an in-plane symmetric vibration and an out-of-plane antisymmetric vibration.[51] As a matter of fact, it is the symmetric in-plane $\upsilon_{as}CH_3$ component that exhibits the intensity in the polarized Raman spectrum, whereas the antisymmetric out-of-plane component is still weak. This has often led to the erroneous assumption that the CH_2 antisymmetric stretching ($\upsilon_{as}CH_2$) should also present in polarized Raman spectra,[22] and consequently, the intense CH_2 Fermi resonance band could be misassigned as $\upsilon_{as}CH_2$. Our gas-phase Raman measurements unambiguously show that the intrinsic Raman intensity of the $\upsilon_{as}CH_2$ modes is, in fact, very low.

With the assignments established for two deuterated samples, the spectra of normal 1-butanol can be easily interpreted. As seen from Figure 4, Raman feature of α-CH_2 and CH_3 groups remains at similar position and intensity from the deuterated to normal 1-butanol. Namely, for normal 1-butanol, the band at 2870 cm^{-1} corresponds to $\upsilon_sC_\alpha H_2$, the two most intense bands at 2879 and 2941 cm^{-1} correspond to the Fermi resonance pairs of υ_sCH_3 and FR-CH_3, and the band at 2963 cm^{-1} corresponds to the overlapping of FR-$C_\alpha H_2$ and $\upsilon_{as}CH_3$. Therefore, the remaining spectral features should originate from the Fermi resonance pairs of the β- and γ-CH_2 groups. By contrasting to the anharmonic predictions in Figure 4a, the bands at 2846 and 2910 cm^{-1} can be attributed to $\upsilon_sC_\beta H_2$ and FR-$C_\beta H_2$ while those at 2856 and 2916 cm^{-1} can be attributed to $\upsilon_sC_\gamma H_2$ and FR-$C_\gamma H_2$. However, unlike the CH_3 and α-CH_2 (Figure 4b,c), the comparison between

https://doi.org/10.1021/acs.jpca.5c08365
J. Phys. Chem. A 2026, 130, 2523−2532

Table 3. Assigned CH_3 and α-CH_2 Fermi Resonance Pairs, Their Unperturbed Fundamental Frequency, and Bending Overtone Estimated by a Two-State Deperturbation Model[a]

molecule	υ_s	υ_{FR}	ΔE	R	ΔE_0	ω	$\upsilon_{fundamental}$[b]	$\upsilon_{overtone}$[b]
$CH_3(CD_2)_3OH$	2879	2938	59	1.26	7	29	2905	2912
$CD_3(CD_2)_2CH_2OH$	2876	2965	89	3.27	47	37	2897	2944

[a]The units are in cm^{-1} for all of the data except for R, which is dimensionless. [b]The estimated unperturbed fundamental frequency and bending overtone of CH_3 and α-CH_2 in the deuterated samples.

experimental and predicted anharmonic spectra shows the discrepancy in the intensity pattern of β- and γ-CH_2 Fermi resonance, especially for β-CH_2, in which the fundamental and overtone intensities are switched. Such an inverse correlation is a consequence of the modulation of the relative contribution of the stretching and bend-overtones during VPT2 calculations. In addition, for the β- and γ-CH_2, the VTP2 calculations overestimated the frequencies of FR-$C_\beta H_2$ and FR-$C_\gamma H_2$ compared to FR-$C_\alpha H_2$ and FR-CH_3. Therefore, it remains a challenge to properly treat the resonant vibrational modes in anharmonic calculations.

From the above assignments, it is evident that Fermi resonance plays a dominant role in reshaping Raman features of 1-butanol in the C−H stretching region. A comparison of four C−H Fermi resonance pairs reveals Raman spectra of 1-butanol are dominated by the terminal CH_3 and α-CH_2 groups, with much weaker contributions from the internal β- and γ-CH_2 groups, as seen from Figure 4a. On the other hand, the comparison with previous measurements on gas-phase Raman spectra of shorter-chain alcohols such as ethanol and 1-propanol reveals that the features of the terminal CH_3 and α-CH_2 groups remain almost unchanged as the chain length increasing,[52,53] whereas that of internal CH_2 groups are highly sensitive to the molecular structure and local environment. Additionally, the gas-phase Raman spectra show that the υ_sCH_3 and $\upsilon_sC_\alpha H_2$ are very close in frequency, and thus the band broadening in the condensed phases can cause them to merge into a single band. However, this integrated band has often been solely attributed to the υ_sCH_2 in liquid Raman measurements, whereas the contribution from the terminal CH_3 was overlooked.[9] These results provide insights into interpreting complex C−H stretching spectra in molecules containing various C−H groups.

In order to obtain more information about the C−H Fermi resonance, we use a two-state perturbation theory to estimate the Fermi resonance coupling constant and the unperturbed fundamental frequency and bending overtone according to the following equations.[54]

$$\Delta E_0 = \Delta E \cdot \frac{R-1}{R+1} \tag{2}$$

$$\omega = \Delta E \cdot \frac{\sqrt{R}}{R+1} \tag{3}$$

where ΔE is energy separation of the observed Fermi resonance pairs and R is their intensity ratio. ΔE_0 is the separation between the zero-order (unperturbed) vibrational states and ω is the coupling constant, assuming that the intrinsic (unperturbed) overtone intensity is negligible. The results are listed in Table 3, where only the parameters of CH_3 and α-CH_2 are shown, whereas for the β- and γ-CH_2, it is difficult to determine the individual spectral contribution due to severe overlap with other vibrational modes in normal 1-butanol. To obtain integral intensity of Fermi resonance pairs, the CH_3 and α-CH_2 stretching spectra in two deuterated samples were deconvoluted by using Lorentz line shape functions, as presented in Figure S5. As seen from Table 3, the Fermi resonance coupling constants of CH_3 and α-CH_2 are 29 and 37 cm^{-1}, respectively, which are lower than about 50 cm^{-1} of NH_2 determined in the hydrogen-bonded complex recently.[55,56]

3.2.3. C−D Stretching Region. Figure 5 presents the polarized Raman spectra of normal 1-butanol and the two

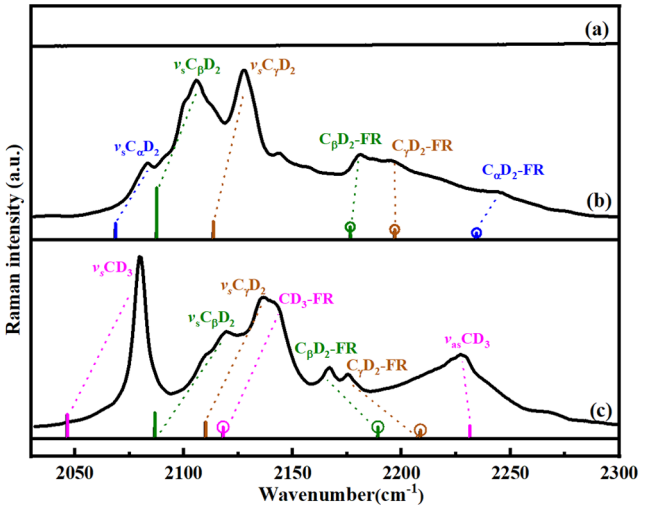

Figure 5. Gas-phase Raman spectra in the C−D stretching region (2000−2300 cm^{-1}) for 1-butanol along with the predicted C−D Fermi resonance pairs by the VPT2 method. (a) $CH_3CH_2CH_2CH_2OH$. (b) $CH_3CD_2CD_2CD_2OH$. (c) $CD_3CD_2CD_2CH_2OH$. Spectral assignments are color-coded as follows: the blue for α-CH_2, the green for β-CH_2, the dark yellow for γ-CH_2, and the pink for CH_3. υ_s: stretching vibration; FR, Fermi resonance. A line with a circle above it denotes the overtone after Fermi resonance interaction. It should be mentioned that for $CD_3CD_2CD_2CH_2OH$, only the calculated symmetric in-plane $\upsilon_{as}CD_3$ is plotted, whereas the antisymmetric out-of-plane $\upsilon_{as}CD_3$ is not.

deuterated isotopologues in the C−D stretching region. As anticipated, no bands are observed in this region for normal 1-butanol (Figure 5a). For $CH_3CD_2CD_2CD_2OH$ in Figure 5b, the spectrum reveals many C−D stretching bands. With the help of the predicted Fermi resonance pairs by the VPT2 method, the bands at 2083 and 2245 cm^{-1} can be assigned to the $\upsilon_sC_\alpha D_2$ and FR-$C_\alpha D_2$, the bands at 2105 and 2181 cm^{-1} correspond to the $\upsilon_sC_\beta D_2$ and FR-$C_\beta D_2$, and the bands at 2127 and 2196 cm^{-1} correspond to the $\upsilon_sC_\gamma D_2$ and FR-$C_\gamma D_2$.

In $CD_3CD_2CD_2CH_2OH$ (Figure 5c), the spectral features associated with the α-CD_2 group are absent, whereas a very intense band appears at 2080 cm^{-1}, which corresponds to the CD_3 symmetric stretching (υ_sCD_3), in agreement with VPT2 calculations. Another two prominent bands at 2119 and 2136

https://doi.org/10.1021/acs.jpca.5c08365
J. Phys. Chem. A 2026, 130, 2523−2532

cm^{-1} can be assigned to $\upsilon_s C_\beta D_2$ and $\upsilon_s C_\gamma D_2$, respectively. A comparison of the spectrum between $CH_3CD_2CD_2CD_2OH$ and $CD_3CD_2CD_2CH_2OH$ reveals a significant broadening of the assigned $\upsilon_s C_\gamma D_2$ accompanied by a distinct shoulder at 2143 cm^{-1}, as seen from Figure 5c. This shoulder should correspond to the CD_3 Fermi resonance partner (FR-CD_3). In addition, an obvious band at 2227 cm^{-1} can be attributed to the CD_3 antisymmetric stretching ($\upsilon_{as}CD_3$) based on the calculations and its characteristic frequency in other deuterated compounds.[23] Notably, the relative intensity of $\upsilon_{as}CD_3$ is significantly enhanced compared to that of $\upsilon_{as}CH_3$. Finally, the remaining bands at 2167 and 2176 cm^{-1} should be from FR-$C_\beta D_2$ and FR-$C_\gamma D_2$ although the anharmonic prediction overestimated the band positions of these two Fermi resonance modes. The parameters such as the Fermi resonance coupling constant are difficult to obtain due to spectral overlapping between the C−D vibrations in two deuterated samples.

4. CONCLUSIONS

The C−H and C−D bending and stretching regions in vibrational spectra contain a wealth of structural information. A precise interpretation of these bands is, therefore, crucial for expanding their analytical utility. In this work, we have employed a sensitive cavity-enhanced Raman instrument to acquire high-resolution gas-phase spectra of 1-butanol and two selectively deuterated isotopologues across the 900−3100 cm^{-1} range, covering both the C−H/C−D bending and stretching regions. The observed spectra were successfully interpreted with the aid of quantum chemical calculations and polarization-resolved measurements.

Our analysis reveals the frequency orders of site-specific C−H bending and stretching spectra in 1-butanol. Also, it shows that vibrational signatures of both the methyl and methylene groups are complicated by Fermi resonance splitting. The deuteration substitution does not cause a mere shift in the position from the C−H to the C−D region, and the relative positions and intensities vary due to differences in the Fermi resonance. Furthermore, a comparative analysis between normal and deuterated 1-butanol shows that the spectral features of the two terminal groups (CH_3 and α-CH_2) exhibit greater similarity and transferability compared to the internal β- and γ-CH_2 groups. In addition, the CH_2 antisymmetric stretching vibrations make a negligible contribution to the gas-phase Raman spectra when contrasting to the CH_3 antisymmetric stretch, clarifying the confusions in previous studies that the CH_2 Fermi resonance modes are often mistaken as $\upsilon_{as}CH_2$. These results establish a reliable foundation for analyzing the structure and dynamics of 1-butanol in various environments. Moreover, they provide fundamental insights that can be applied to the interpretation of C−H and C−D spectra in other molecular systems containing alkyl chains, which are ubiquitous structural motifs in organic and biological chemistry. Future work will focus on the development of more sophisticated theoretical models to accurately simulate the anharmonic interactions, particularly Fermi resonance in the C−H and C−D stretching regions of alcohols like 1-butanol.

■ ASSOCIATED CONTENT

Supporting Information

The Supporting Information is available free of charge at https://pubs.acs.org/doi/10.1021/acs.jpca.5c08365.

Figures S1−S3 plotted the calculated harmonic frequencies and Raman activities for the first five conformers of normal 1-butanol and two deuterated samples in the C−H/C−D bending and stretching regions from 900 to 3100 cm^{-1} along with experimental spectra; Figure S4 displays the atomic displacement vector of in-phase CH_2 twisting mode in normal 1-butanol; Figure S5 shows the fitted gas-phase Raman spectra of two deuterated 1-butanol in the C−H stretching region using Lorentz line shape functions (PDF)

■ AUTHOR INFORMATION

Corresponding Author

Yan Tan − *Hefei National Research Center of Physical Sciences at the Microscale, University of Science and Technology of China, Hefei 230026, China;* orcid.org/0000-0003-3073-3152; Email: tanyan@ustc.edu.cn

Authors

Yuanqin Yu − *School of Physics, Anhui University, Hefei 230601, China;* orcid.org/0000-0001-7647-8404

Chongyan Shi − *School of Physics, Anhui University, Hefei 230601, China;* orcid.org/0009-0006-3358-7380

Qingying Yang − *Hefei National Research Center of Physical Sciences at the Microscale, University of Science and Technology of China, Hefei 230026, China*

Shuiming Hu − *Hefei National Research Center of Physical Sciences at the Microscale, University of Science and Technology of China, Hefei 230026, China;* orcid.org/0000-0002-1565-8468

Complete contact information is available at: https://pubs.acs.org/10.1021/acs.jpca.5c08365

Notes

The authors declare no competing financial interest.

■ ACKNOWLEDGMENTS

This work was jointly supported by the National Natural Science Foundation of China (Grants Nos. 21873002 and 12393825) and Innovation Program for Quantum Science and Technology (Grant Nos. 2021ZD0303102 and 2021ZD0303304).

■ REFERENCES

(1) Shen, H. Y.; Chen, N.; You, A.; Yu, Y. Q.; Zhou, X. G.; Zhang, R.; Liu, S. L. Structural features of liquid DMSO from temperature-dependent Raman spectroscopy and theoretical calculations. *Chin. J. Chem. Phys.* **2024**, *37* (6), 763−768.

(2) Wang, Z. Q.; Dan, G. Y.; Zhang, R. T.; Ma, L.; Lin, K. Coupling and decoupling CH stretching vibration of methylene and methine in serine conformers. *Spectrochim. Acta, Part A* **2023**, *285*, No. 121829.

(3) Singh, S.; Huang, Q. R.; Tan, J. A.; Kuo, J. L.; Patwari, G. N. Ab initio anharmonic analysis of complex vibrational spectra of phenylacetylene and fluorophenylacetylenes in the acetylenic and aromatic C-H stretching region. *J. Chem. Phys.* **2023**, *159* (10), No. 104302.

(4) Lacinbala, O.; Feraud, G.; Vincent, J.; Pino, T. Aromatic and Acetylenic C-H or C-D Stretching Bands Anharmonicity Detection of Phenylacetylene by UV Laser-Induced Vibrational Emission. *J. Phys. Chem. A* **2022**, *126*, 4891−4901.

(5) Yadav, S.; Banik, S.; Prasad, M. D. Understanding of the C-H stretch region of infra-red spectroscopy: an analysis of the final state wavefunctions. *Phys. Chem. Chem. Phys.* **2021**, *23* (15), 9176−9188.
(6) Kiefer, J.; Wagenfeld, S.; Kerlé, D. Chain length effects on the vibrational structure and molecular interactions in the liquid normal alkyl alcohols. *Spectrochim. Acta, Part A* **2018**, *189*, 57−65.
(7) Fischer, S. A.; Ueltschi, T. W.; El-Khoury, P. Z.; Mifflin, A. L.; Hess, W. P.; Wang, H. F.; Cramer, C. J.; Govind, N. Infrared and Raman Spectroscopy from Ab Initio Molecular Dynamics and Static Normal Mode Analysis: The C-H Region of DMSO as a Case Study. *J. Phys. Chem. B* **2016**, *120* (8), 1429−1436.
(8) Ashraf, M. A.; Metz, R. B. Structure and vibrational spectroscopy of complexes of Al+ and Al2+ with ethane. *J. Chem. Phys.* **2025**, *162* (15), No. 154302.
(9) Hellerer, T.; Axäng, C.; Brackmann, C.; Hillertz, P.; Pilon, M.; Enejder, A. Monitoring of lipid storage in Caenorhabditis elegans using coherent anti-Stokes Raman scattering (CARS) microscopy. *Proc. Natl. Acad. Sci. U.S.A.* **2007**, *104* (37), 14658−14663.
(10) Mori, W.; Wang, L.; Sato, Y.; Morita, A. Development of quadrupole susceptibility automatic calculator in sum frequency generation spectroscopy and application to methyl C-H vibrations. *J. Chem. Phys.* **2020**, *153* (17), No. 174705.
(11) Lu, R.; Gan, W.; Wu, B. H.; Zhang, Z.; Guo, Y.; Wang, H. F. C-H stretching vibrations of methyl, methylene and methine groups at the vapor/alcohol (n = 1−8) interfaces. *J. Phys. Chem. B* **2005**, *109* (29), 14118−14129.
(12) Liu, A. A.; Liu, S.; Zhang, R. D.; Ren, Z. F. Spectral Identification of Methanol on TiO2(110) Surfaces with Sum Frequency Generation in the C-H Stretching Region. *J. Phys. Chem. C* **2015**, *119* (41), 23486−23494.
(13) Batignani, G.; Ferrante, C.; Fumero, G.; et al. Femtosecond stimulated Raman spectroscopy. *Nat. Rev. Methods Primers* **2024**, *4* (1), No. 34, DOI: 10.1038/s43586-024-00314-6.
(14) Mitoli, D.; Maul, J.; Erba, A. First-Principles Anharmonic Infrared and Raman Vibrational Spectra of Materials: Fermi Resonance in Dry Ice. *J. Phys. Chem. Lett.* **2024**, *15* (4), 888−894.
(15) Šebek, J.; Knaanie, R.; Albee, B.; Potma, E. O.; Gerber, R. B. Spectroscopy of the C-H Stretching Vibrational Band in Selected Organic Molecules. *J. Phys. Chem. A* **2013**, *117* (32), 7442−7452.
(16) Šebek, J.; Pele, L.; Potma, E. O.; Gerber, R. B. Raman spectra of long chain hydrocarbons: anharmonic calculations, experiment and implications for imaging of biomembranes. *Phys. Chem. Chem. Phys.* **2011**, *13* (28), 12724−12733.
(17) Sibert, E. L., III; Tabor, D. P.; Kidwell, N. M.; Dean, J. C.; Zwier, T. S. Fermi Resonance Effects in the Vibrational Spectroscopy of Methyl and Methoxy Groups. *J. Phys. Chem. A* **2014**, *118* (47), 11272−11281.
(18) Huang, Q. R.; Endo, T.; Mishra, S.; Zhang, B. B.; Chen, L. W.; Fujii, A.; Jiang, L.; Patwari, G. N.; Matsuda, Y.; Kuo, J. L. Understanding Fermi resonances in the complex vibrational spectra of the methyl groups in methylamines. *Phys. Chem. Chem. Phys.* **2021**, *23* (6), 3739−3747.
(19) Zhang, B. B.; Huang, Q. R.; Jiang, S. K.; Chen, L. W.; Hsu, P. J.; Wang, C.; Hao, C.; Kong, X. T.; Dai, D. X.; Yang, X. M.; Kuo, J. L.; Jiang, L. Infrared spectra of neutral dimethylamine clusters: An infrared-vacuum ultraviolet spectroscopic and anharmonic vibrational calculation study. *J. Chem. Phys.* **2019**, *150* (6), No. 064317.
(20) Ullah, N.; Jiao, Z. R.; Bai, J. L.; Wang, Z. Q.; Zhang, R. T.; Ma, L.; Lin, K. Removing Fermi resonance through deuterated molecules with single C-H bond in C-H stretching region of Raman spectra. *Chin. J. Chem. Phys.* **2024**, *37* (6), 783−791.
(21) Bernath, P. F.; Sibert, E. L. Cyclohexane Vibrations: High-Resolution Spectra and Anharmonic Local Mode Calculations. *J. Phys. Chem. A* **2020**, *124* (48), 9991−10000.
(22) Zaytseva, Y. V.; Surovtsev, N. Raman scattering in protonated and deuterated 1,2-dipalmitoyl-sn-glycero-3-phosphatidylcholine (DPPC): Indicators of conformational and lateral orders. *Spectrochim. Acta, Part A* **2022**, *267*, No. 120583.
(23) Okotrub, K. A.; Shamaeva, D.; Surovtsev, N. Raman spectra of deuterated hydrocarbons for labeling applications. *J. Raman Spectrosc.* **2022**, *53* (2), 297−309.
(24) Tyrode, E.; Hedberg, J. A Comparative Study of the CD and CH Stretching Spectral Regions of Typical Surfactants Systems Using VSFS: Orientation Analysis of the Terminal CH3 and CD3 Groups. *J. Phys. Chem. C* **2012**, *116* (1), 1080−1091.
(25) Di Martino, R. M. C.; Maxwell, B. D.; Pirali, T. Deuterium in drug discovery: progress, opportunities and challenges. *Nat. Rev. Drug Discovery* **2023**, *22* (7), 562−584.
(26) Wang, Z.; Pakoulev, A.; Dlott, D. D. Watching vibrational energy transfer in liquids with atomic spatial resolution. *Science* **2002**, *296* (5576), 2201−2203.
(27) Kataoka, S.; Cremer, P. S. Probing molecular structure at interfaces for comparison with bulk solution behavior: Water/2-propanol mixtures monitored by vibrational sum frequency spectroscopy. *J. Am. Chem. Soc.* **2006**, *128* (16), 5516−5522.
(28) Li, Y. H.; Yang, X. L.; Yu, Y. Q.; Zhou, X. G.; Zhang, R.; Sun, J.; Liu, S. L. Dependence of Intramolecular Hydrogen Bond on Conformational Flexibility in Linear Aminoalcohols. *J. Phys. Chem. A* **2023**, *127* (43), 9013−9021.
(29) You, A.; Li, Y. H.; Yang, X. L.; Shen, H. Y.; Yu, Y. Q.; Zhou, X. G.; Zhang, R.; Liu, S. L. Conformational equilibrium of aminoethanol in the gas phase and in solution driven by intra- and intermolecular interactions and solvent polarity. *J. Chem. Phys.* **2025**, *162* (16), No. 164309.
(30) Hartwig, B.; Suhm, M. A. Subtle hydrogen bonds: benchmarking with OH stretching fundamentals of vicinal diols in the gas phase. *Phys. Chem. Chem. Phys.* **2021**, *23* (38), 21623−21640.
(31) Lwin, E.; Gölz, M. J.; Lüttschwager, N. O. B.; Suhm, M. A.; Käser, S.; Andreichev, V.; Brandes, M. A.; Meuwly, M. Rotational, vibrational, conformational and diastereomeric dimer cooling of aminoalcohols in soft supersonic expansions and the monohydrate of dimethylaminoethanol. *Phys. Chem. Chem. Phys.* **2025**, *27* (34), 17692−17703.
(32) Yang, Q.-y.; Tan, Y.; Qu, Z.-h.; Sun, Y.; Liu, A.-w.; Hu, S.-m. Multiple Gas Detection by Cavity-Enhanced Raman Spectroscopy with Sub-ppm Sensitivity. *Anal. Chem.* **2023**, *95* (13), 5652−5660.
(33) Wassermann, T. N.; Zielke, P.; Lee, J. J.; Cezard, C.; Suhm, M. A. Structural preferences, argon nanocoating, and dimerization of n-alkanols as revealed by OH stretching spectroscopy in supersonic jets. *J. Phys. Chem. A* **2007**, *111* (31), 7437−48.
(34) Doroshenko, I.; Vaskivskyi, Y.; Chernolevska, Y. Structural transformations in solid and liquid n-butanol from FTIR spectroscopy. *Mol. Cryst. Liq. Cryst.* **2020**, *697* (1), 11−19.
(35) Doroshenko, I.; Vaskivsky, Y.; Chernolevskaya, Y.; Doroshenko, O. Conformational composition of 1-butanol in matrix isolation. *Low Temp. Phys.* **2021**, *47* (4), 318−324.
(36) Pal, D.; Chakraborty, S. A matrix isolation infrared spectroscopic study of thermal isomerisation of 1-butanol. *Chem. Phys. Lett.* **2021**, *775*, No. 138671.
(37) Crowder, G.; Townsend, M. J. Vibrational spectra of 1-butanol. *J. Mol. Struct.* **1977**, *42*, 27−30.
(38) Ohno, K.; Yoshida, H.; Watanabe, H.; Fujita, T.; Matsuura, H. Conformational study of 1-butanol by the combined use of vibrational spectroscopy and ab initio molecular orbital calculations. *J. Phys. Chem. A* **1994**, *98* (28), 6924−6930.
(39) Czarnecki, M. A.; Wojtkow, D.; Haufa, K. Rotational isomerism of butanols:: Infrared, near-infrared and DFT study. *Chem. Phys. Lett.* **2006**, *431* (4−6), 294−299.
(40) Grabska, J.; Bec, K. B.; Ozaki, Y.; Huck, C. W. Temperature Drift of Conformational Equilibria of Butyl Alcohols Studied by Near-Infrared Spectroscopy and Fully Anharmonic DFT. *J. Phys. Chem. A* **2017**, *121* (9), 1950−1961.
(41) Yang, T. T.; Zhou, D. L.; Ye, S.; Li, X. Y.; Li, H. R.; Feng, Y.; Jiang, Z. F.; Yang, L.; Ye, K.; Shen, Y. X.; Jiang, S.; Feng, S.; Zhang, G. Z.; Huang, Y.; Wang, S.; Jiang, J. Catalytic Structure Design by AI Generating with Spectroscopic Descriptors. *J. Am. Chem. Soc.* **2023**, *145* (49), 26817−26823.

(42) Zou, Z. H.; Zhang, Y. J.; Liang, L. J.; Wei, M. Z.; Leng, J. C.; Jiang, J.; Luo, Y.; Hu, W. A deep learning model for predicting selected organic molecular spectra. *Nat. Comput. Sci.* **2023**, *3* (11), 957.
(43) Frisch, M. J.; Trucks, G. W.; Schlegel, H. B.; Scuseria, G. E.; Robb, M. A.; Cheeseman, J. R.; Scalmani, G.; Barone, V.; Petersson, G. A.; Nakatsuji, H.; Li, X.; Caricato, M.; Marenich, A. V.; Bloino, J.; Janesko, B. G.; Gomperts, R.; Mennucci, B.; Hratchian, H. P.; Ortiz, J. V.; Izmaylov, A. F.; Sonnenberg, J. L.; Williams; Ding, F.; Lipparini, F.; Egidi, F.; Goings, J.; Peng, B.; Petrone, A.; Henderson, T.; Ranasinghe, D.; Zakrzewski, V. G.; Gao, J.; Rega, N.; Zheng, G.; Liang, W.; Hada, M.; Ehara, M.; Toyota, K.; Fukuda, R.; Hasegawa, J.; Ishida, M.; Nakajima, T.; Honda, Y.; Kitao, O.; Nakai, H.; Vreven, T.; Throssell, K.; Montgomery, J. A., Jr.; Peralta, J. E.; Ogliaro, F.; Bearpark, M. J.; Heyd, J. J.; Brothers, E. N.; Kudin, K. N.; Staroverov, V. N.; Keith, T. A.; Kobayashi, R.; Normand, J.; Raghavachari, K.; Rendell, A. P.; Burant, J. C.; Iyengar, S. S.; Tomasi, J.; Cossi, M.; Millam, J. M.; Klene, M.; Adamo, C.; Cammi, R.; Ochterski, J. W.; Martin, R. L.; Morokuma, K.; Farkas, O.; Foresman, J. B.; Fox, D. J. *Gaussian 16*, revision C.01; Wallingford, CT, 2016.
(44) Tian, L. Molclus Program Version 1.3.5., 2016. http://www.keinsci.com/research/molclus.html.
(45) Lu, T.; Chen, Q. Shermo: A general code for calculating molecular thermochemistry properties. *Comput. Theor. Chem.* **2021**, *1200*, No. 113249.
(46) Barone, V. Anharmonic vibrational properties by a fully automated second-order perturbative approach. *J. Chem. Phys.* **2005**, *122* (1), No. 014108.
(47) Boerio, F. J.; Koenig, J. L. Raman Scattering in Crystalline Polyethylene. *J. Chem. Phys.* **1970**, *52* (7), 3425−3431.
(48) Torres-Hernández, F.; Pinillos, P.; Li, W. Q.; Saragi, R. T.; Camiruaga, A.; Juanes, M.; Usabiaga, I.; Lesarri, A.; Fernández, J. A. Competition between O-H and S-H Intermolecular Interactions in Conformationally Complex Systems: The 2-Phenylethanethiol and 2-Phenylethanol Dimers. *J. Phys. Chem. Lett.* **2024**, *15* (21), 5674−5680.
(49) Chen, L.; Zhu, W. D.; Lin, K.; Hu, N. Y.; Yu, Y. Q.; Zhou, X. G.; Yuan, L. F.; Hu, S. M.; Luo, Y. Identification of Alcohol Conformers by Raman Spectra in the C-H Stretching Region. *J. Phys. Chem. A* **2015**, *119* (13), 3209−3217.
(50) Yao, B. T.; Bai, J. L.; Li, X. Y.; Dong, Y. X.; Zhang, R. T.; Wang, Z. Q.; Ma, L.; Lin, K. Conformational structure and intermolecular interaction of phenylalanine by Raman spectroscopy in the C-H stretching region. *Spectrochim. Acta, Part A* **2026**, *348*, No. 127137.
(51) Yu, Y. Q.; Wang, Y. X.; Lin, K.; Hu, N. Y.; Zhou, X. G.; Liu, S. L. Complete Raman Spectral Assignment of Methanol in the C-H Stretching Region. *J. Phys. Chem. A* **2013**, *117* (21), 4377−4384.
(52) Yu, Y. Q.; Wang, Y. X.; Lin, K.; Zhou, X. G.; Liu, S. L.; Sun, J. New spectral assignment of n-propanol in the C-H stretching region. *J. Raman Spectrosc.* **2016**, *47* (11), 1385−1393.
(53) Yu, Y.; Lin, K.; Zhou, X.; Wang, H.; Liu, S.; Ma, X. New C-H stretching vibrational spectral features in the Raman spectra of gaseous and liquid ethanol. *J. Phys. Chem. C* **2007**, *111* (25), 8971−8978.
(54) Herzberg, G. Molecular Spectra and Molecular Structure II. In *Infrared and Raman Spectra of Polyatomic Molecules*; van, D., Ed.; Nostrand Company Inc.: NJ, 1945.
(55) Mishra, S.; Kuo, J. L.; Patwari, G. N. Hydrogen bond induced enhancement of Fermi resonances in N-H•••N hydrogen bonded complexes of anilines. *Phys. Chem. Chem. Phys.* **2018**, *20* (33), 21557−21566.
(56) Mishra, S.; Nguyen, H. Q.; Huang, Q. R.; Lin, C. K.; Kuo, E. L.; Patwari, G. N. Vibrational spectroscopic signatures of hydrogen bond induced NH stretch-bend Fermi-resonance in amines: The methyl-amine clusters and other N-HN hydrogen-bonded complexes. *J. Chem. Phys.* **2020**, *153* (19), No. 194301.

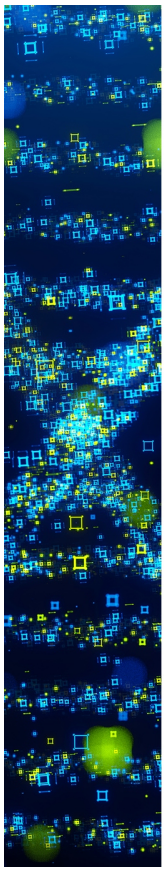
CAS BIOFINDER DISCOVERY PLATFORM™
STOP DIGGING THROUGH DATA —START MAKING DISCOVERIES
CAS BioFinder helps you find the right biological insights in seconds
Start your search
CAS
A division of the American Chemical Society

https://doi.org/10.1021/acs.jpca.5c08365
J. Phys. Chem. A 2026, 130, 2523−2532